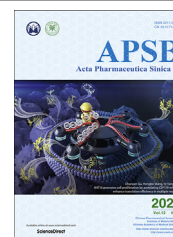




Chinese Pharmaceutical Association  
Institute of Materia Medica, Chinese Academy of Medical Sciences

Acta Pharmaceutica Sinica B

[www.elsevier.com/locate/apsb](http://www.elsevier.com/locate/apsb)  
[www.sciencedirect.com](http://www.sciencedirect.com)



## ORIGINAL ARTICLE

# A temporo-spatial pharmacometabolomics method to characterize pharmacokinetics and pharmacodynamics in the brain microregions by using ambient mass spectrometry imaging



Dan Liu<sup>a,b</sup>, Jianpeng Huang<sup>a</sup>, Shanshan Gao<sup>a</sup>, Hongtao Jin<sup>c,d</sup>,  
Jiuming He<sup>a,d,\*</sup>

<sup>a</sup>State Key Laboratory of Bioactive Substance and Function of Natural Medicines, Institute of Materia Medica, Chinese Academy of Medical Sciences and Peking Union Medical College, Beijing 100050, China

<sup>b</sup>Department of Clinical Pharmacy, First People's Hospital of Huaihua, Huaihua 418000, China

<sup>c</sup>New Drug Safety Evaluation Center, Institute of Materia Medica, Chinese Academy of Medical Sciences and Peking Union Medical College, Beijing 100050, China

<sup>d</sup>NMPA Key Laboratory for Safety Research and Evaluation of Innovative Drug, Beijing 100050, China

Received 18 January 2022; received in revised form 10 March 2022; accepted 20 March 2022

## KEY WORDS

Pharmacometabolomics;  
Pharmacokinetics;  
Pharmacodynamics;  
Mass spectrometry  
imaging;  
Antipsychotic drug

**Abstract** The brain is the most advanced organ with various complex structural and functional microregions. It is often challenging to understand what and where the molecular events would occur for a given drug treatment in the brain. Herein, a temporo-spatial pharmacometabolomics method was proposed based on ambient mass spectrometry imaging and was applied to evaluate the microregional effect of olanzapine (OLZ) on brain tissue and demonstrate its effectiveness in characterizing the microregional pharmacokinetics and pharmacodynamics of OLZ for improved understanding of the molecular mechanism of drugs acting on the microregions of the brain. It accurately and simultaneously illustrated the levels dynamics and microregional distribution of various substances, including exogenous drugs and its metabolites, as well as endogenous functional metabolites from complicated brain tissue. The targeted imaging analysis of the prototype drug and its metabolites presented the absorption, distribution, metabolism, and excretion characteristics of the drug itself. Moreover, the endogenous functional metabolites were identified along with the associated therapeutic and adverse effects of the drug, which can reflect the pharmacodynamics effect on the microregional brain. Therefore, this method is

\*Corresponding author. Tel./fax: +86 10 63165218.

E-mail address: [hejiuming@imm.ac.cn](mailto:hejiuming@imm.ac.cn) (Jiuming He).

Peer review under responsibility of Chinese Pharmaceutical Association and Institute of Materia Medica, Chinese Academy of Medical Sciences.

<https://doi.org/10.1016/j.apsb.2022.03.018>

2211-3835 © 2022 Chinese Pharmaceutical Association and Institute of Materia Medica, Chinese Academy of Medical Sciences. Production and hosting by Elsevier B.V. This is an open access article under the CC BY-NC-ND license (<http://creativecommons.org/licenses/by-nc-nd/4.0/>).

significant in elucidating and understanding the molecular mechanism of central nervous system drugs at the temporo and spatial metabolic level of system biology.

© 2022 Chinese Pharmaceutical Association and Institute of Materia Medica, Chinese Academy of Medical Sciences. Production and hosting by Elsevier B.V. This is an open access article under the CC BY-NC-ND license (<http://creativecommons.org/licenses/by-nc-nd/4.0/>).

## 1. Introduction

The central nervous system (CNS) has an intricate and fragile structure with high interconnectivity and interaction among numerous microregions of the brain. The brain has the most complicated and finest structure and function, which regulates all aspects of behavior, language, thinking, memory, movement, and emotions<sup>1</sup>. Based on the neural structure, chemical characteristics, and connectivity, it can be subdivided into numerous microregions, such as the cerebral cortex, midbrain, pons, medulla oblongata, hippocampus, and hypothalamus<sup>2</sup>. The functional differences in metabolic enzymes, receptors, ligands, transporters, and blood flow in the brain microregions<sup>3</sup> cause differences in spatial distribution and efficacy of drugs. Additionally, the brain contains a variety of endogenous functional metabolites that are unevenly distributed in the different microregions<sup>4</sup>. Therefore, it is very challenging to develop CNS drugs and elucidate what and where the molecular events would occur for a given drug treatment, as most CNS drugs exert effects only after entering the brain. For drug development, it is crucial to understand the pharmacokinetics (absorption, distribution, metabolism, and excretion) and pharmacodynamics of the drug<sup>5</sup>. Developing novel technologies may provide new opportunities and promote the research of innovative drugs<sup>6,7</sup>.

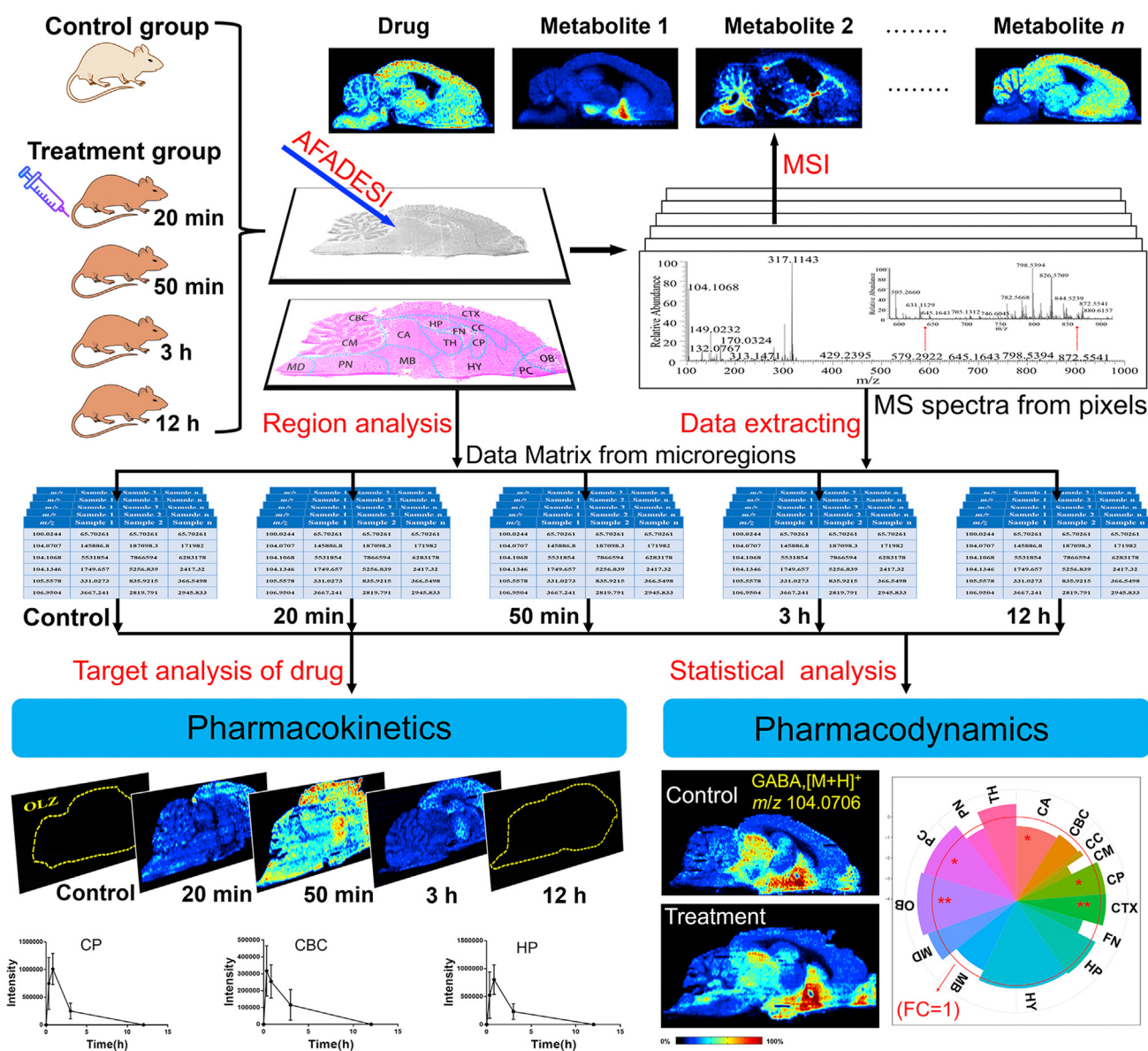
In the recent years, liquid chromatography mass spectrometry (LC–MS) based pharmacometabolomics has been proven to be a powerful tool in identifying an organism's metabolic response following drug administration through an investigation of the overall changes of metabolites in the body. LC–MS can provide information on drug metabolism, drug action-associated alteration in the endogenous metabolic pathway, and can correlate drug pharmacokinetics, pharmacodynamics, and *in vivo* effects to elucidate the molecular mechanisms of drug effects and toxicity<sup>8–10</sup>. LC–MS-based pharmacometabolomics analyzes body fluids, such as blood and urine, and reflects the average metabolic level of various tissues and organs in the body. Tissues and organs are the focal site of most diseases as well as drug action, with the brain being the target site for CNS diseases. Thus, information about the *in situ* distribution of drugs in the brain is significant to evaluate drug efficacy, toxicology, and pharmacokinetics<sup>11</sup>.

At present, the common techniques used to study the brain include several types of functional brain imaging, such as functional magnetic resonance imaging (fMRI)<sup>12</sup> and positron emission tomography (PET)<sup>13,14</sup>, and structural brain imaging such as magnetic resonance imaging (MRI)<sup>15</sup>, computerized tomography (CT)<sup>16</sup>, single photon emission computed tomography (SPECT)<sup>17</sup>, and other CT technologies. Although structural and functional imaging technology plays an increasingly important role in disease research and CNS drug development, these technologies only provide images of the structure of brain tissue without analysis at the molecular level<sup>18</sup>, with low spatial resolution and with limited types of substances that can be

monitored<sup>19</sup>. On the other hand, intracerebral drug analysis often uses tissue homogenates or microdialysis sampling based high-performance liquid chromatography mass spectrometry (HPLC–MS) technology. The pre-processing of tissue sample is invasive and can damage the brain tissue microregions. The obtained results thus reflect only the average metabolic level of the sampled microregion<sup>20,21</sup> with no information on the spatial distribution of the molecule throughout the brain.

Mass spectrometry imaging (MSI) has received great attention and has been rapidly developed in recent years. Compared with other imaging technologies (histochemical labeling, immunofluorescence, MRI, PET, whole body autoradiography, etc.), it is a molecular imaging technology and does not require complicated pre-processing and specific chemical labeling<sup>22–25</sup>. MSI has become a powerful tool with high-throughput, high-sensitivity, and high-resolution that detects the qualitative and spatial distribution information of known or unknown molecules including peptides, proteins, endogenous metabolites, or exogenous drugs<sup>26–28</sup>. MSI has been applied to reveal asymmetrical spatial distribution of lipid metabolites from bisphenol S induced nephrotoxicity<sup>29</sup>, aristolochic acid-induced nephrotoxicity, tissue-specific metabolic reprogramming in diabetic nephropathy<sup>30,31</sup>, to determine glucose metabolism in different regions of the brain<sup>32</sup>, and to reveal the biologically relevant correlation between cholesterol and other metabolites in the brain<sup>33</sup>. In particular, we developed air flow-assisted desorption electrospray ionization (AFADESI)-MSI technology with high sensitivity, wide metabolites coverage, which can map thousands of structure-specific and functional metabolites in an untargeted analysis<sup>34</sup>. This technology is applied in many areas, such as *in situ* biomarker discovery for cancer diagnosis<sup>35</sup>, tumor metabolism research<sup>36</sup>, and elucidating mechanism of drug action<sup>37</sup>. A series of MSI techniques such as matrix-assisted laser desorption ionization (MALDI) MSI<sup>38,39</sup>, liquid extraction surface analysis tandem mass spectrometry (LESA–MS/MS)<sup>40</sup>, and desorption electrospray ionization (DESI) MS<sup>41</sup> have been reported to quantify OLZ from bio-tissue. There is still an urgent need for an imaging application method that can simultaneously characterize the pharmacokinetics and pharmacodynamics of brain microregions to facilitate CNS drug development.

Herein, we developed a temporo-spatial pharmacometabolomics method, based on the air flow-assisted desorption electrospray ionization mass spectrometry imaging (AFADESI-MSI) system coupled with a high-resolution mass spectrometer, which can provide high-coverage molecular profile and microregional distribution information. The research strategy is shown in Scheme 1. This method was validated with a case study on the temporo-spatial changing of the levels of olanzapine (OLZ), a CNS drug used in clinical practice, and the endogenous metabolites in the rat brain over the period of administration and the analysis of pharmacokinetics and pharmacodynamics of the drug in the brain microregions.



**Scheme 1** Strategy and workflow of the proposed temporo-spatial pharmacometabolomics method to characterize the microregional pharmacokinetics and pharmacodynamics of CNS drugs in the brain.

Overall, this method was successful at demonstrating the temporo-spatial characteristics of OLZ and its action-related metabolites and provided new insights into the molecular mechanism of action of CNS drugs.

## 2. Materials and methods

### 2.1. Chemicals and reagents

HPLC-grade acetonitrile was purchased from Merck (Darmstadt, Germany). Purified water was obtained from Wahaha (Hangzhou, China). Formic acid was provided by Millipore (Merck, Darmstadt, Germany), and olanzapine (OLZ) bulk drug powder (Supporting Information Fig. S1) was purchased from Shanghai Yuan Ye Biotechnology Co., Ltd., China.

### 2.2. Animal experiments

The animal experiments were conducted with the approval of the Animal Ethical Committee at the Institute of Materia Medical, Chinese Academy of Medical Science, and Peking Union Medical College (Beijing, China). Male Sprague–Dawley rats (weighing 180–200 g) were purchased from Vital River Laboratory Animal Technology Company (Beijing, China). The animals were maintained for a week with unlimited standard food and water at a constant room temperature of  $22 \pm 2$  °C and 45%–55% humidity under a 12 h light/dark cycle. The rats were randomly divided into two groups: treatment group and control group. The treatment group was further divided into 4 groups of 3 animals each, which were orally administered OLZ solutions (50 mg/mL) prepared by mixing OLZ powder with saline. Rats were euthanized with high concentrations of ether at 20 min, 50 min, 3 h, and 12 h after administration

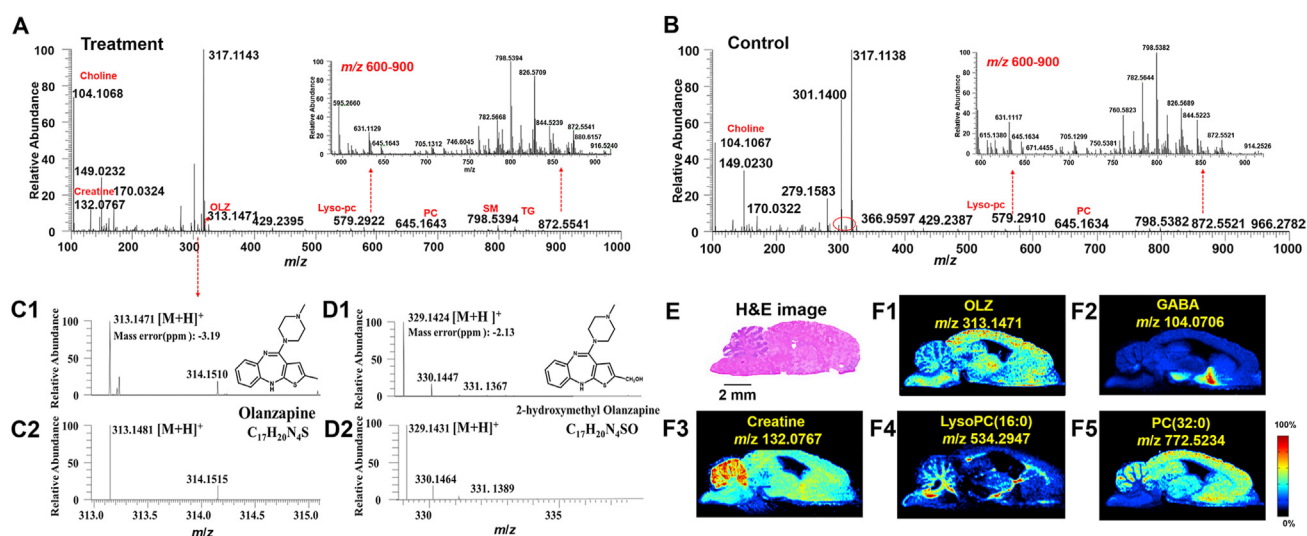


**Figure 1** Imaging results for exogenous drug and endogenous metabolites obtained using AFADESI-MSI from brain tissue section. The representative mass spectra acquired using AFADESI-MSI from treatment (A) and control groups (B) brain tissue section in positive ion mode. C1 and D1 are experimental mass spectra of olanzapine (OLZ) and its metabolite, 2-hydroxymethyl OLZ, respectively. C2 and D2 are the calculated isotopic peaks of OLZ and 2-hydroxymethyl OLZ, respectively. (E) represents the hematoxylin-eosin (H&E) staining of sections of the brain. Scale bar = 2 mm. (F1)–(F5) show ion images of OLZ,  $\gamma$ -aminobutyric acid (GABA), Creatine, LysoPC (16:0), PC (32:0), respectively.

( $n = 3$  at each time point). The control group ( $n = 3$ ) were given an equal volume of saline by the gavage route. The whole brain of each animal was collected and stored at  $-80^{\circ}\text{C}$  until sectioning. The general brain perfusion with saline for blood–brain barrier (BBB) permeable drugs was not performed to keep the original metabolic status for metabolic analysis and to avoid the loss of unstable endogenous metabolites, such as neurotransmitters (NTs).

### 2.3. Preparation of brain tissue sections

The brain tissue sections were sliced to consecutive sagittal slices of  $15\ \mu\text{m}$  using a Leica CM1860 Cryostat Microtome (Leica Microsystems Ltd., Germany) at  $-20^{\circ}\text{C}$ , and the tissue sections were thaw-mounted on positively charged desorption plates (Thermo Scientific, CA, USA) and stored in closed slice boxes at  $-80^{\circ}\text{C}$  until further analysis. The frozen slices were dried in a vacuum desiccator at  $-20^{\circ}\text{C}$  for 1 h and then kept at room temperature for another 1 h before AFADESI-MSI analysis. Meanwhile, the serial brain tissue sections were fixed with 4% paraformaldehyde and subjected to hematoxylin–eosin (H&E) staining.

### 2.4. AFADESI-MSI analysis

The MSI experiments were performed using an AFADESI-MSI platform, which consisted of a home-built ambient AFADESI ion source and a Q Orbitrap Mass Analyzer (Q Exactive, Thermo Fisher Scientific, CA, USA)<sup>42,43</sup>. The key parameters included spray voltage, ion transfer tube voltage, solvent flow rate, and transporting gas flow rate. The SC100 Series Stepper Motor (Beijing Optical Century Instrument Co., Beijing, China) was used to control the movement of the brain tissue sections. The parameters were set in the self-designed control platform program. The experiments were achieved by continuously scanning the brain tissue surface in the  $x$  direction at a constant velocity of  $160\ \mu\text{m/s}$ , with a vertical step separation of  $200\ \mu\text{m}$  between adjacent lines in the  $y$  direction. A mixed solution of acetonitrile:water (8:2,  $v/v$ ) was used as the optimized spray solvent with a flow rate of  $5\ \mu\text{L/min}$ . The MSI

analysis was performed in positive and negative ion modes on a Q-Exactive mass spectrometer. A detailed parameter setting is shown in [Supporting Information Table S1](#).

### 2.5. Data processing and statistical analysis

The raw data from the AFADESI-MS analysis was converted to cdf format files using Xcalibur 2.3 (Thermo Scientific, USA) and then imported into the custom-developed graphical software MassImager (Version 1.0, Chemmind Technologies Co., Ltd., Beijing, China) for ion image reconstruction<sup>44</sup>. After background subtraction, each section was normalized to the sample total ion chromatograms (TIC) value using MassImager, and the ion images were finally presented using the TIC normalized intensity threshold. MS profiles from the microregions of brain were precisely extracted from the MSI data by matching ion images with high-spatial resolution H&E staining images of the adjacent brain section, and each brain microregion profile was delineated and calculated 3 times from the subregions to reduce error. The average ion intensity of the microregion was calculated to generate separated two-dimensional data matrixes ( $m/z$ , ion intensity) in the.txt format. The mass tolerance for peak pick and background subtraction was set to  $0.005\ \text{Da}$ , and the proportional coefficient  $k$  was set to 1. Thereafter, the.txt file was imported into Markerview 1.2.1 (AB SCIEX, USA) for peak alignment and isotope ion deletion. Multivariate statistical analysis was carried out using SIMCA-P 14.0 (Umetrics AB, Umeå, Sweden), which included principal component analysis (PCA) and orthogonal partial least squares discriminant analysis (OPLS-DA). The metabolic profiles of the control and treatment groups were compared by performing supervised multivariate OPLS-DA to achieve the maximal separation. The variable importance in projection (VIP) value was calculated for each ion to indicate their contribution to the OPLS-DA model. Analysis of variance (ANOVA) was used to compare the differences between the control and treatment groups.  $P < 0.05$  indicates a significant difference relative to the control group. Therefore, variables, which satisfied the following conditions, were considered to be potential



metabolites: variables with a VIP value  $\geq 1.0$  and  $P < 0.05$  in independent  $t$ -test. Finally, the isotope and adduct ions were deleted according to the corresponding extracted ion chromatograms (XICs). The area under the curve (AUC) was calculated using GraphPad Prism 6.0. software.

2.6. Analyte identification

The adducted ions of potential biomarkers were compared with the public databases including the Human Metabolome Database ([www.hmdb.ca](http://www.hmdb.ca)), Metlin (<https://metlin.scripps.edu>), MassBank (<http://www.massbank.jp/>), and LIPID MAPS ([www.lipidmaps.org](http://www.lipidmaps.org)), using exact molecular weights with a mass error of less than 5 ppm and isotope patterns, combined with the isotopic

abundance of high-resolution mass spectra that provide the elemental composition and likelihood list of the endogenous metabolites<sup>45</sup>. Then, the high-resolution MS/MS spectra were used for further identification. The high-resolution tandem MS experiments were performed on an orbitrap mass spectrometer (Q Exactive, Thermo Scientific, Bremen, Germany) and conducted directly from brain sections to obtain structural information based on the interpretation of the metabolites' fragmentation patterns and database searches. For *in situ* AFADESI-MS/MS analysis, the resolution of the MS/MS acquisition was set to 70,000 with an AGC value of 5e6 and a maximum injection time of 200 ms. The ions of interest were considered as targets, and the NCE values were set to 25%, 35%, and 45% in the targeted MS2 scan mode.

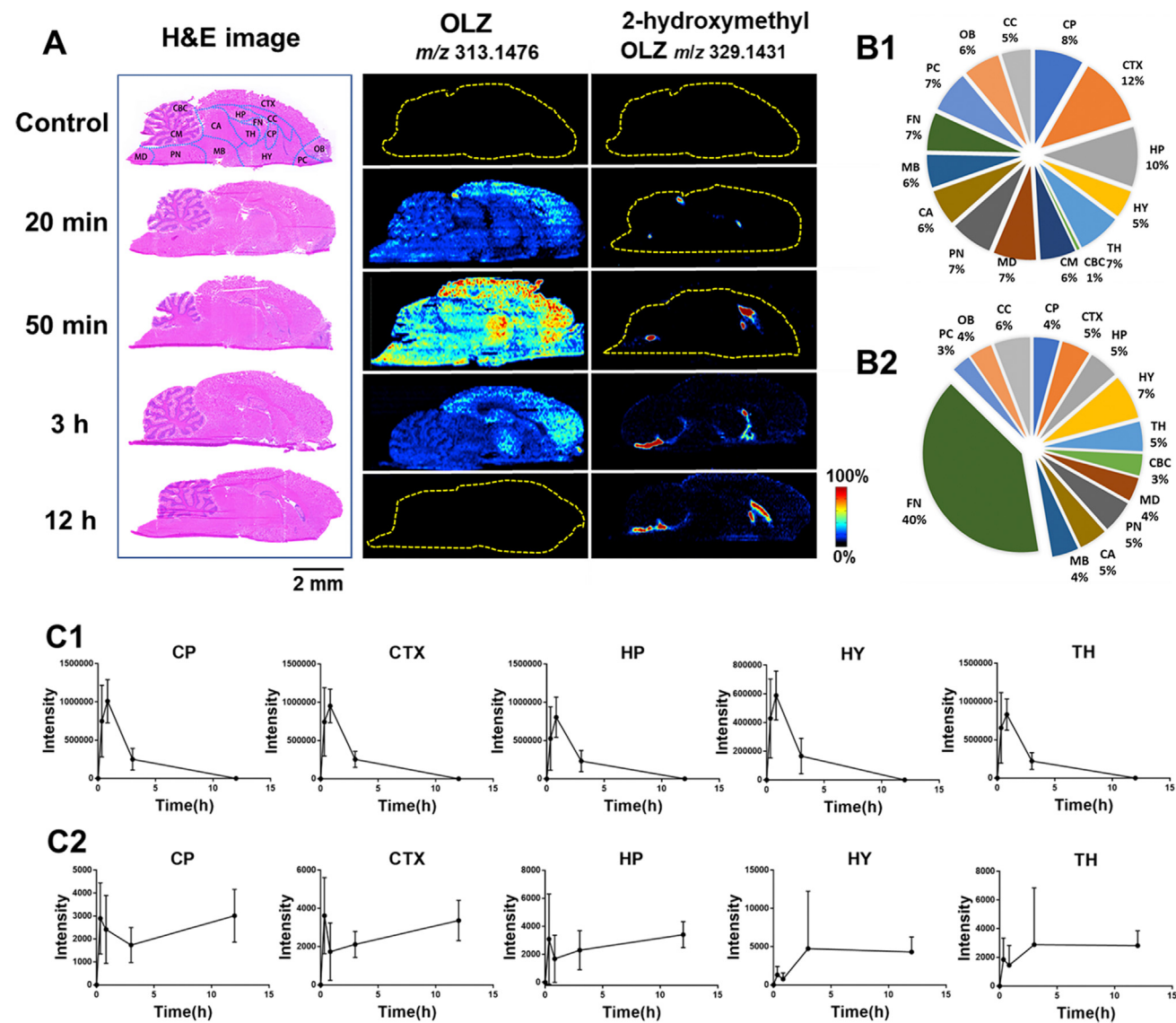


**Figure 2** Temporo-spatial alteration of OLZ and 2-hydroxymethyl OLZ in brain microregions. (A) MS images of OLZ and 2-hydroxymethyl OLZ in brain tissue section acquired using AFADESI-MSI. (B1, B2) The percentage of AUC in OLZ and 2-hydroxymethyl OLZ in different brain microregions. (C1, C2) The relative intensity changes of OLZ and 2-hydroxymethyl OLZ in the different brain microregions with the time. Data are presented as means  $\pm$  standard deviation (SD),  $n = 3$ . CP: caudate putamen, CTX: cerebral cortex, HP: hippocampus, HY: hypothalamus, TH: thalamus, CBC: cerebellar cortex, CM: cerebellar medulla, MD: medulla, PN: pons, CA: cerebral aqueduct, MB: middle brain, FN: fornix, PC: piriform cortex, OB: olfactory bulb, and CC: corpus callosum.

### 3. Results and discussion

#### 3.1. Mapping the drug and endogenous metabolites in the rat brain

AFADESI-MSI is a powerful imaging tool used to map the exogenous compounds and endogenous metabolites from the brain

tissue section. The representative mass spectra acquired using AFADESI-MSI from treatment and control groups brain tissue sections in positive ion mode is shown in Fig. 1A, B and that in negative ion mode is shown in Fig. S1A and B. The average mass spectrum showed that the endogenous metabolite ions detected in different brain microregions are diverse and the intensities differed greatly. In the low mass range of 100–500 Da, amino acids,

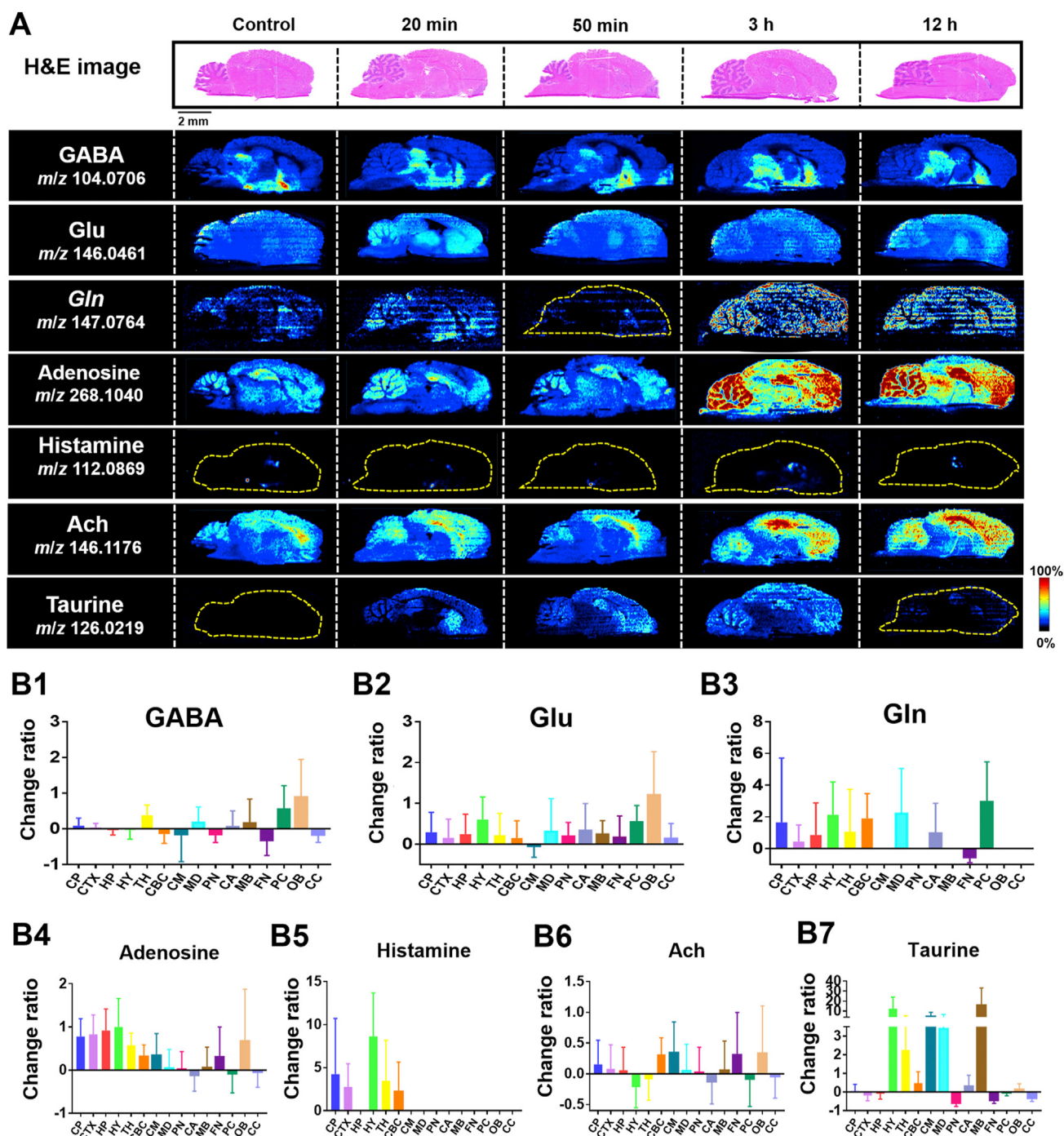


**Figure 3** Drug effect on the distribution and AUC change ratio for NTs in brain. (A) represents the images of H&E-stained brain sections followed by the distribution of NTs in the brain acquired by AFADESI-MSI. (B1–B7) show the AUC change ratio of NTs. AUC change ratio = (AUC after drug–AUC before drug)/AUC before drug. AUC change ratio >0 indicates an up-regulated status. AUC change ratio <0 indicates a down-regulated status. The larger absolute values of the AUC change ratio represent greater up-regulation or down-regulation with the drug action or effect.

nucleosides, nucleotides, small molecular organic acids, and some background ions could be detected; in the high mass range of 500–1000 Da, some lipid components, including sphingomyelin (SM), phosphatidylethanolamine (PE), phosphatidylcholine (PC), and some lysophosphatidylcholine (LysoPC) were detected. Components such as  $\gamma$ -aminobutyric acid (GABA,  $m/z$  104.0706), creatine ( $m/z$  132.0765), carnitine ( $m/z$  162.1120), acetylcarnitine ( $m/z$  204.1231), and phosphatidylcholine ( $m/z$  786.5258) were detected in the positive ion mode, while glutamic acid (Glu,  $m/z$  146.0461), fatty acid (18:1) ( $m/z$  281.2486), fatty acid (20:4) ( $m/z$  303.2330), ascorbic acid ( $m/z$  175.0276), and phosphatidylinositol (PI,  $m/z$  885.5502) were detected in the negative ion mode. Ion images of these metabolites could be observed visually with their uneven microregional distribution information and the prominent structural profile of brain tissue (Fig. 1F1–F5, Fig. S1D1–S1D5) was characterized. The prototype drug OLZ and its metabolite 2-hydroxymethyl OLZ were detected in the positive ion mode, which was confirmed by their accurate mass assignment and identical isotopic peak shape. The results are shown in Fig. 1C1 and D1, and the theoretical matching isotopic peak is shown in Fig. 1C2 and D2. These results indicated that this non-targeted MSI method can simultaneously map the exogenous drugs and endogenous metabolites in a single experiment and can obtain their spatial distribution characteristics and microregional abundance variation.

### 3.2. Temporo-spatial changes in OLZ and its metabolite in the brain

OLZ is a drug used to treat schizophrenia, with the brain being its main target organ. To explore the distribution of drugs in various functional microregions of the brain over the time of administration, the rat brain tissues of the treatment and control rats were collected at 20 min, 50 min, 3 h, and 12 h after drug administration for MSI analysis. As shown in Fig. 2A, 15 microregions of interests were focused on the caudate putamen (CP), cerebral cortex (CTX), hippocampus (HP), hypothalamus (HY), thalamus (TH), cerebellar cortex (CBC), cerebellar medulla (CM), medulla (MD), pons (PN), cerebral aqueduct (CA), middle brain (MB), fornix (FN), piriform cortex (PC), olfactory bulb (OB), and corpus callosum (CC). The microstructure of the rat brain samples is shown in Supporting Information Fig. S2.

From the MS images of the brain sections (Fig. 2A), the spatial distributions of the prototype drug OLZ and its metabolite 2-hydroxymethyl OLZ were detected. These results showed that OLZ can readily penetrate the BBB, largely dispersed in the ventricles and brain parenchymal tissue but not uniformly distributed in all microregions of the brain, to act on the CNS. It was found that OLZ is distributed mainly in the CTX 20 min after administration. After 50 min, the levels of OLZ increased significantly. With the progression of time, the drug signal in the brain quickly dropped below the imaging detection limit. Simultaneously, it was found that 2-hydroxymethyl OLZ, mainly distributed in the FN, had a different distribution pattern in the various microregions than that of OLZ. There was a significant increase in abundance of 2-hydroxymethyl OLZ 20 min after administration, and the metabolite was still present in high concentrations after 12 h of administration. Furthermore, the percentage of AUC of OLZ (Fig. 2B1) was similar in different microregions of the brain, except in CBC that was smaller, which indicates that the degree of drug absorption is similar in brain microregions, and less in the CBC. The percentage of AUC of

2-hydroxymethyl OLZ (Fig. 2B2) in FN was the largest, indicating that the exposure was the largest in the FN microregion. The metabolic exposure was similar in the other microregions. Additionally, the changes in relative intensity of OLZ in the different brain microregions with time (Fig. 2C1 and Supporting Information Fig. S3A) showed that in the CBC, CM, MD, PN, CA, MB, PC, OB, and CC, the highest level of OLZ was reached at 20 min after administration and then gradually decreased, while in the CP, CTX, HP, HY, TH, and FN, OLZ reached the highest level at 50 min after administration. Fig. 2C2 and Fig. S3B show that the level of 2-hydroxymethyl OLZ increased with time lapsed after administration in 12 of the microregions of the brain and increased dramatically in the PN.

These results indicated that the rate of drug absorption, distribution, and metabolism differ in various microregions of the brain, suggesting microregional effects on pharmacokinetics. It also demonstrated that the proposed temporo-spatial pharmacometabolomics method based on AFADESI-MSI has the ability to simultaneously illustrate changes in the levels of and spatial distribution of drugs and their metabolites in the complicated microregions of the brain.

### 3.3. Microregional regulation of NTs by OLZ

OLZ is a first-line drug used in the clinical setting to treat schizophrenia. It acts mainly by regulating NTs. The known mechanism of action is by blocking the dopamine D2 receptor or the serotonin 2A receptor<sup>46,47</sup>. However, the microregional effect and the molecular mechanism of action of OLZ are still unclear. Therefore, we further analyzed the temporo-spatial changes of NTs that are closely related to the physiological activity of OLZ. As shown in Fig. 3A, a variety of NTs, such as GABA, Glu, glutamine (Gln), and adenosine, were detected. The AUC change ratio of NTs is shown in Fig. 3B1–B7. Supporting Information Figs. S4–S10 reflects the relative intensity changes of NTs in the different brain microregions with time. This mode of targeted analysis of functional metabolites from the non-targeted metabolic data has the advantage of not requiring predetermined parameters for the detection of metabolites.

GABA is a NT in the CNS that inhibits the nerve center, induces sleep, calmness, and prevents elevated body temperature by reducing neuronal activity to produce anti-anxiety effects<sup>48</sup>. The ion image showed that GABA ( $m/z$  104.0706) was mainly distributed in the HY and was down-regulated after drug intervention. In the HY, the level of GABA decreased 20 min from drug administration and increased after 20 min up to 3 h. After 3 h from administration, the level of GABA gradually decreased (Fig. S4). The changed AUC ratio in the HY was  $-0.03$ -fold (Fig. 3B1). The minor variation in ratio indicates that GABA was lightly regulated after drug intervention in the HY. However, simultaneously, significant upregulation after drug intervention was observed in OB and PC, combined with the AUC changed ratio. Glu, a major neurotransmitter in the CNS, has an excitatory effect on nerve cells and can excite cells to death<sup>49</sup>. The temporal and spatial dynamic patterns of Glu and its metabolite, Gln, present a relatively consistent change trend in microregions after drug intervention (Figs. S5 and S6). Adenosine is widely distributed in the CNS and is considered to be an excitatory and inhibitory neurotransmitter in the brain<sup>50,51</sup>. It was unevenly distributed in various microregions, and the high levels of adenosine in the HP and HY increased significantly after 3 h from administration (Fig. S7), indicating that the up-regulation of adenosine would be



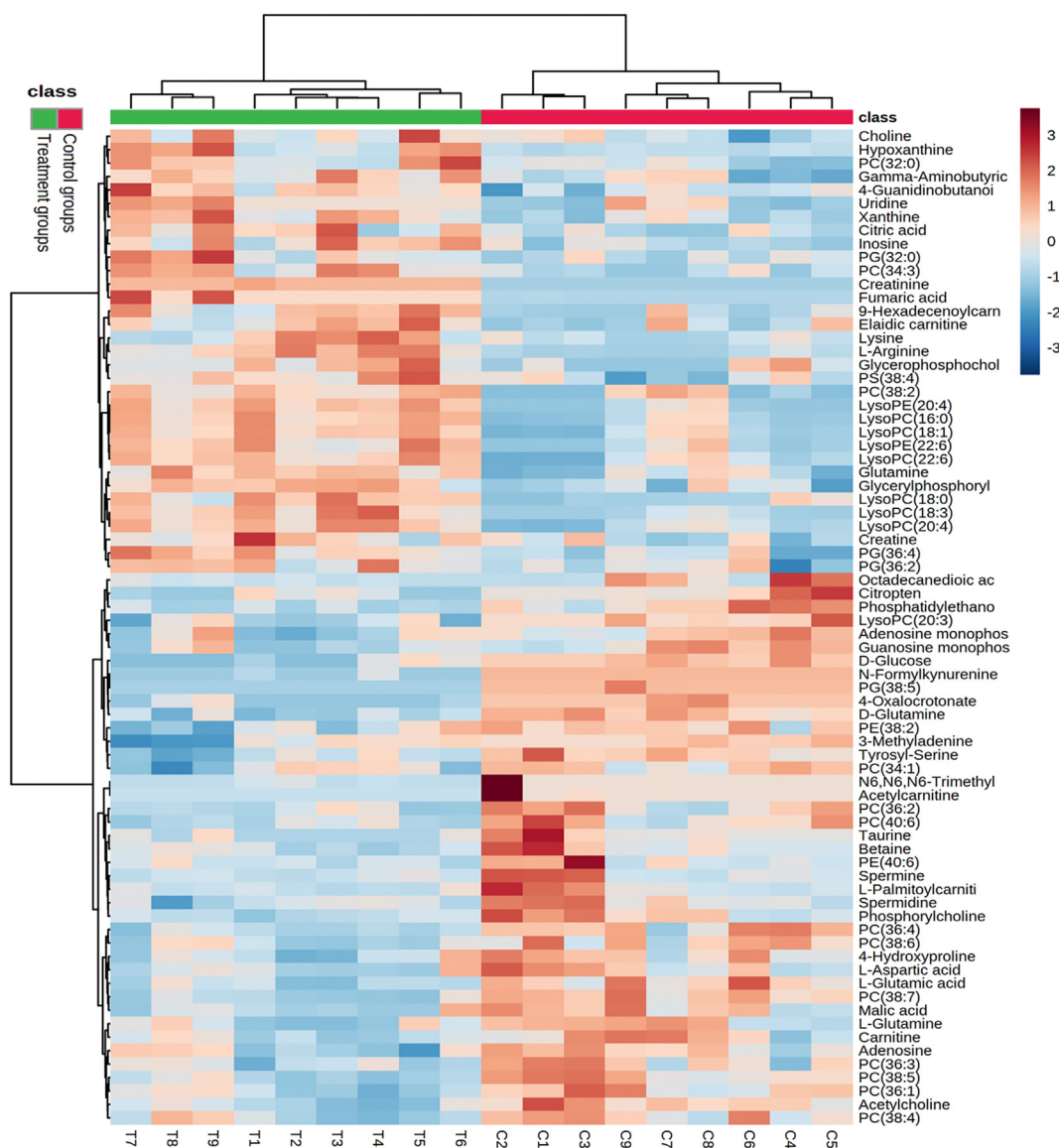


**Figure 4** Hierarchical cluster analysis (HCA) of identified differential metabolites in control and treatment groups. The row on the right lists the metabolites, the column on the top indicates class (green: treatment groups and red: control groups), and the column on the bottom indicates sample ID (T: treatment groups sample and C: control groups sample). The metabolites were clustered, and shades of red and blue represent high expression levels and low expression levels, respectively.

more obvious when the drug accumulates. Histamine, as a central neurotransmitter, participates in the regulation of cognitive memory, sleep and wakefulness, diet, and other functions<sup>52,53</sup>. It was specifically distributed in the CP, CTX, HY, and TH and was up-regulated during drug action (Fig. S8). The effect of acetylcholine (ACh) on central neurons is mainly through the excitement and activation of brain nerve conduction function to enhance the brain's memory capacity<sup>54</sup>. ACh is highly distributed in the CTX and tends to increase with a prolonged administration (Fig. S9). Taurine promotes the growth and development of the nervous system and cell proliferation and differentiation<sup>55</sup>. It was observed that the levels of taurine increased after OLZ intervention (Fig. S10).

The results of the targeted imaging analysis of the above-mentioned NTs demonstrated that this method can detect the spatial distribution and variation in an abundance of prototype

drugs, their metabolites, and endogenous metabolites related to the mechanism of action of CNS drugs. This is significant in elucidating the mechanism of action of CNS drugs and understanding schizophrenia and related diseases.

### 3.4. Microregional metabolic regulation with drug intervention by OLZ

Endogenous metabolic changes in tissues and organs can reflect the effect of drug stimulation. To explore the microregional metabolic effects after drug intervention, the molecular profile of endogenous metabolites and the distribution information of their dynamic changes were investigated with pharmacometabolomic testing in various brain microregions. Three brain tissue samples from each group of treatment and control rats taken 50 min after OLZ and saline administration, respectively, were selected for



Then, the discriminating metabolites were imported into MetaboAnalyst 5.0 (<https://www.metaboanalyst.ca/>) and combined with Kyoto Encyclopedia of Genes and Genomes PATHWAY Database (<https://www.genome.jp/kegg/pathway.html>) to perform metabolic pathway matching analysis, facilitating the

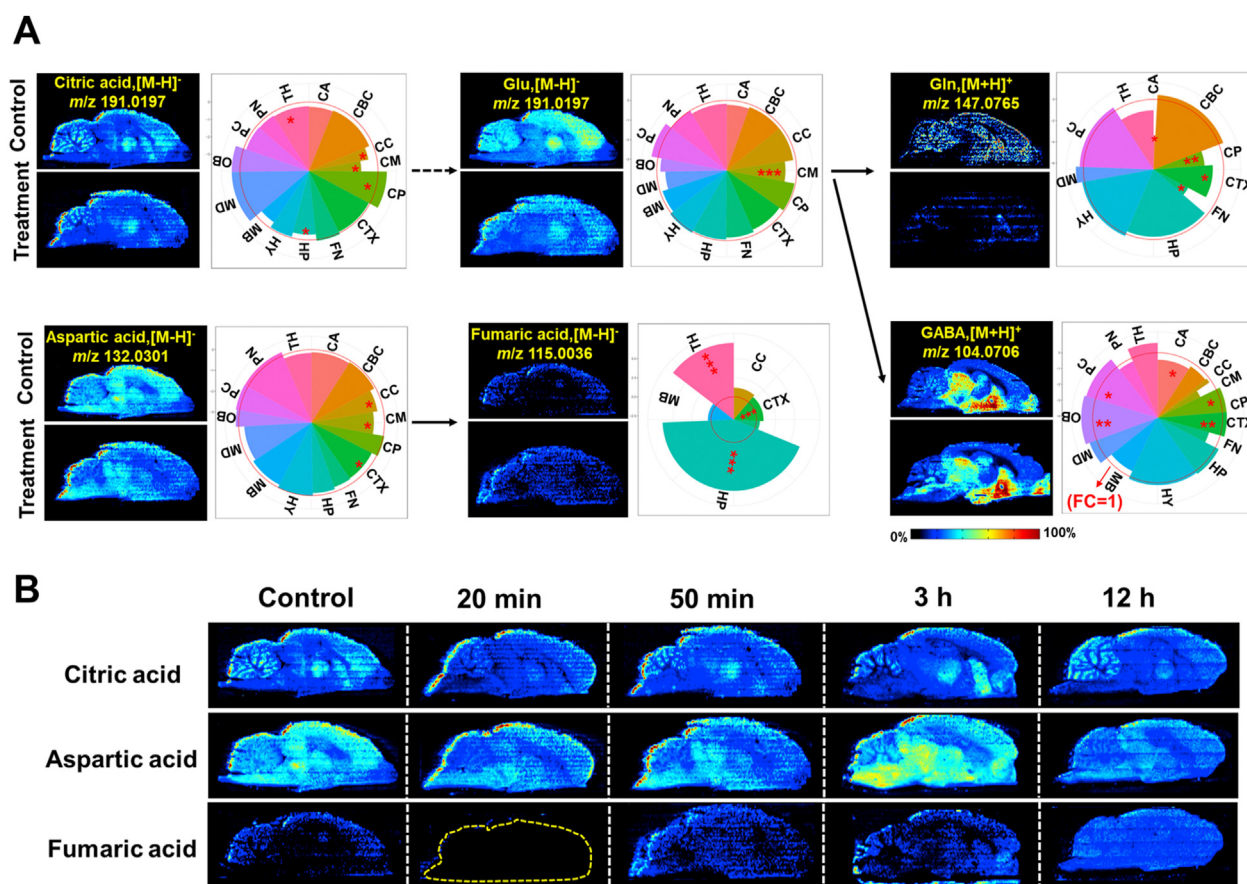


**Figure 5** Temporo-spatial distribution of metabolites of the alanine, aspartate, and glutamate metabolism pathway. (A) Spatial distribution and changes of metabolites involved in the alanine, aspartate, and glutamate metabolism pathway in the treatment (50 min after dosing) and control groups. (B) MS images of metabolites of the alanine, aspartate, and glutamate metabolism pathways in brain tissue section acquired using AFADESI-MSI. Statistical analysis of the metabolome data extracted from control and treatment groups (50 min) in different brain microregions. (means  $\pm$  SD),  $n = 3$ . \* $P < 0.05$ , \*\* $P < 0.01$  and \*\*\* $P < 0.001$ . The red circle in the pie chart represents the conversion of  $\log_2(1)$  equal to 0 when the fold change of metabolite before and after administration is 1 ( $FC = 1$ ). The sector outside the red circle represents the fold change greater than 1 ( $FC > 1$ ) and indicates this metabolite with up-regulation after drug intervention in this microregion, while the sector inside the red circle represents the fold change less than 1 ( $FC < 1$ ) and indicates this metabolite with down-regulation after drug intervention in this microregion. The distance of the radius of the sector from the red circle represents the degree of fold change. Outside the red circle, a larger radius of the sector represents more pronounced up-regulation, and within the red circle, a smaller radius of the sector represents more significant down-regulation. The size of the rounding angle represents the relative abundance in the microregion; the larger the rounding angle, the greater the relative abundance.

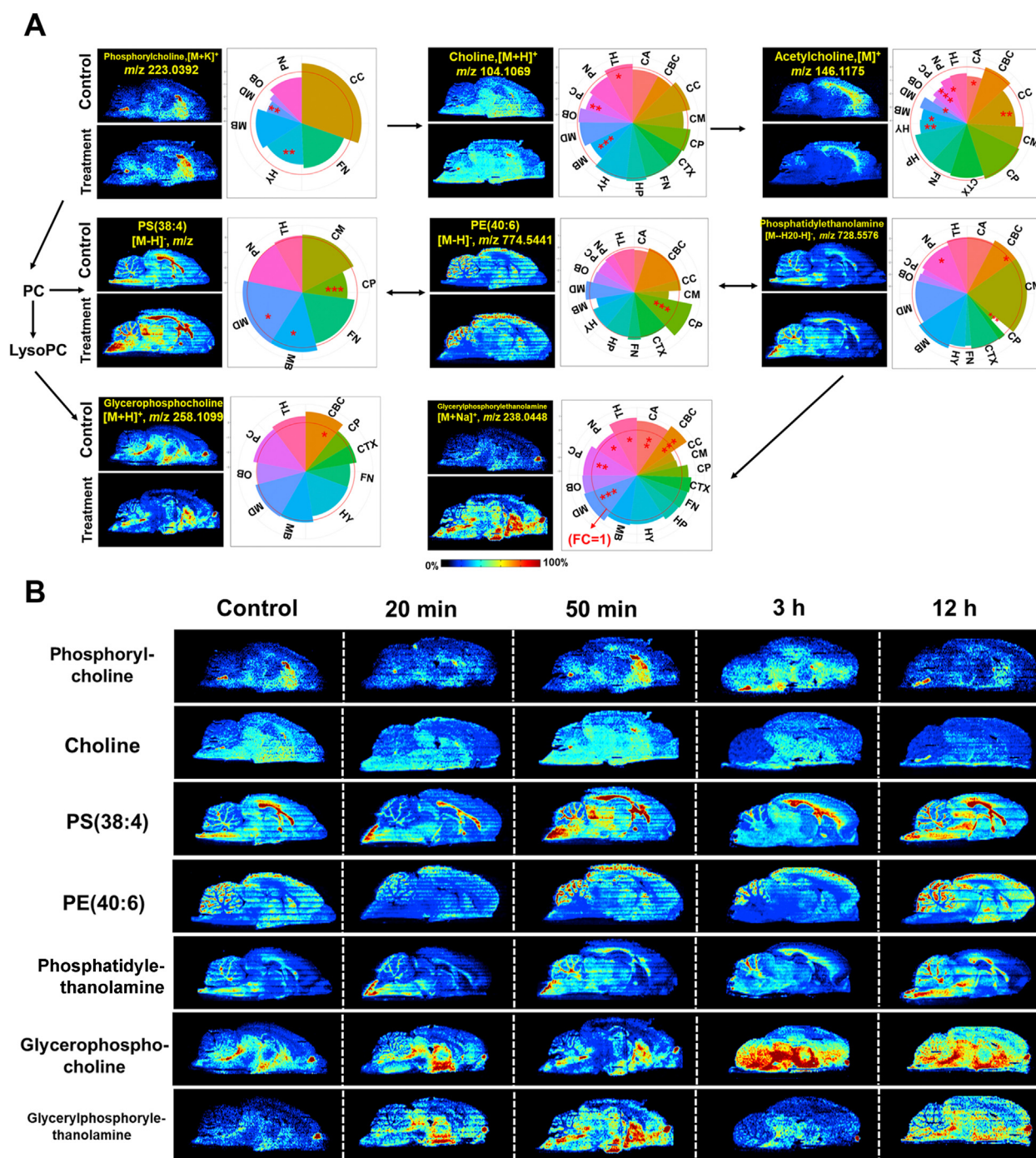


**Figure 6** Temporo-spatial distribution of metabolites of the glycerophospholipid metabolism pathway. (A) Spatial distribution and changes of metabolites involved in the glycerophospholipid metabolism pathway in the treatment (50 min after dosing) and control groups. (B) MS images of metabolites of the glycerophospholipid metabolism pathway in brain tissue section acquired using AFADESI-MSI. Statistical analysis was performed using Student's *t*-test. \**P* < 0.05, \*\**P* < 0.01 and \*\*\**P* < 0.001.

discovery of altered metabolic pathways<sup>56</sup>. This analysis suggested that multiple metabolic pathways were significantly dysregulated (Supporting Information Fig. S15 and Table S3). The impact-value threshold calculated from the pathway topology analysis was set to 0.10. Seven metabolic pathways significantly perturbed between treatment and control groups were identified, which included alanine, aspartate and glutamate metabolism, D-glutamine and D-glutamate metabolism, taurine and hypotaurine

metabolism, starch and sucrose metabolism, glycerophospholipid metabolism, arginine and proline metabolism, arginine biosynthesis, purine metabolism, and citrate cycle (TCA cycle). To more accurately explore the changes in metabolic levels associated with the mechanism of action of OLZ, we focused on the abnormal metabolic pathways of alanine, aspartate, glutamate, and glycerophospholipid metabolism with parameters of large pathway impact (PI) and small Raw *P*.

### 3.4.1. Disturbance in alanine, aspartate, and glutamate metabolism

Glu is synthesized from Gln by glutamine synthetase (GLS). Its clearance can prevent neuronal excitotoxicity caused by excessive activation of glutamate receptors<sup>57</sup>. Gln can generate Glu through GLS and enter the tricarboxylic acid (TCA) cycle to provide energy for cell life activities<sup>58</sup>. An abnormal Glu–Gln cycle plays an important role in the pathophysiological process of schizophrenia<sup>59</sup>. The temporo-spatial distributions of metabolites of the alanine, aspartate, and glutamate metabolism pathway are shown in Fig. 5. The AUC change ratio of metabolites is shown in Supporting Information Fig. S16. From the spatial distribution maps along with drug intervention, it was observed that the proportion of the key metabolites varied in different microregions of the brain and their fold change after drug intervention showed trends of up-regulation or down-regulation. Among them, citric acid was evenly distributed in most of the microregions of the brain; the level was significantly increased compared with those in control. It is well known that citric acid is an intermediate of the TCA cycle, which is the final metabolic pathway for the complete oxidation of sugar, fat, and protein in the body and is the main way for the body to obtain energy<sup>60,61</sup>. This result suggested that the level of citric acid was up-regulated after drug intervention, indicating that drug intervention accelerated the metabolism of TCA cycle and provided more energy to the body. Glu was also evenly distributed in various microregions, showing a down-regulation after drug intervention. Its metabolism produced Gln and GABA, which were up-regulated mainly in the HY and in multiple microregions of the brain, respectively.

According to the above pathway analysis and the metabolic glutamate decarboxylase (GAD) enzyme reaction, it could be speculated that OLZ directly activated GAD to promote the synthesis of GABA<sup>62</sup>. GABA increases the activity of hexokinase in glycolysis, thereby accelerating the metabolism of glucose, increasing the supply of blood and oxygen to the brain, and promoting sleep<sup>63–65</sup>. The distribution of glucose in brain is presented in Supporting Information Fig. S17. The spatial distribution shows that glucose is distributed in all microregions of the brain but primarily in the OB and PC after administration. There was a significant increase in glucose levels 20 min after administration.

### 3.4.2. Disturbance of the glycerophospholipid metabolism pathway

Lipids have a variety of biological functions, including material transportation, energy metabolism, information recognition and transmission, cell development, differentiation, and apoptosis<sup>66</sup>. Glycerophospholipids help to control liver lipid metabolism, promote memory, enhance immunity, and delay aging<sup>67</sup>. Lipids may participate in the regulation of schizophrenia by regulating the integrity of the myelin sheath and neuronal function<sup>68</sup>. Lipid metabolism is associated with brain cognitive function<sup>69</sup>. Several studies have confirmed that independent phospholipase A2 $\beta$  (iPLA2 $\beta$ ) is a novel ferroptosis regulator, and the associated mutations may be involved in the pathological process of Parkinson's disease, which is mainly related to the insufficient repair of oxidized phospholipids<sup>70,71</sup>. The temporo-spatial distribution of metabolites of the glycerophospholipid metabolism pathway is shown in Fig. 6. The AUC change ratio of metabolites is shown in Supporting Information Fig. S18. The highest levels of phosphorylcholine were seen in the CC and were significantly upregulated. PS (38:4) was significantly downregulated in the CP and upregulated in the CM, MB, and MD. Glycerophosphocholine showed an up-regulation in the CBC.

Upregulated PE (40:6) was observed in the CP. Phosphatidylethanolamine was significantly downregulated in the CP, and the levels were the highest in the CM. Glycerolphosphorylethanolamine showed an upregulation in most microregions. The results of this study showed that after the administration of OLZ, most of the lipids showed an up-regulation in majority of the microregions. OLZ has metabolic side effects in clinical applications, such as weight gain, dyslipidemia, hypertriglyceridemia, and insulin resistance. These experimental results proved that the upregulation of lipid metabolism may contribute to these side effects during treatment with OLZ, and further confirmation is needed about the biological significance of more lipid substances.

These results demonstrated that the temporo-spatial pharmacometabolomics method was effective in identifying the endogenous molecular effectors associated with drug action. The data revealed targeted and non-targeted metabolic alterations with variation in their abundance while also illustrating their spatial distribution information to show the precise location in the microregions targeted by the drug. This method is, therefore, significant in understanding the pharmacodynamics of CNS drugs.

## 4. Conclusions

We developed a temporo-spatial pharmacometabolomics method to characterize the pharmacokinetics and pharmacodynamics of CNS drugs in the brain using ambient MSI. Compared with LC–MS based pharmacometabolomics, AFADESI-MSI based temporo-spatial pharmacometabolomics has the advantage of detecting the static level changes of endogenous and exogenous substances and providing dynamic time-dependency trends and spatial distribution information in the different microregions of the brain, accurately presenting *in situ* and microregional molecular events. Therefore, correlation of pharmacokinetics and pharmacodynamics with metabolic pathways at the level of systems biology is conducive for obtaining critical information for deeper understanding of the molecular mechanisms of drug action.

The temporo-spatial pharmacometabolomics method developed in this study was applied to evaluate the microregional effect of OLZ on brain tissue and demonstrate its effectiveness in characterizing the microregional pharmacokinetics and pharmacodynamics of CNS drugs crossing the blood–brain-barrier. This method clearly presented the pharmacokinetics of the prototype drug and its metabolite 2-hydroxymethyl OLZ in different microregions of the rat brain. Moreover, the microregional pharmacodynamics of OLZ was illustrated through mapping metabolic pathways. It was found that some NTs, including GABA, adenosine, and histamine, displayed multiple metabolic pathways related to drug intervention. Furthermore, the regulation of aspartate, glutamate, and the glycerophospholipid metabolism pathway could be associated with the therapeutic and adverse effects observed with the clinical usage of OLZ, which provides critical information for understanding the molecular mechanism of its action.

In summary, the temporo-spatial pharmacometabolomics method provided a comprehensive and effective tool for elucidating the *in situ* pharmacokinetics and pharmacodynamics of CNS drugs.

## Acknowledgments

This study was supported by the National Natural Science Foundation of China (Grant Nos. 81773678 and 81974500) and the



CAMS Innovation Fund for Medical Sciences (CIFMS, 2021-I2M-1-026, China).

### Author contributions

Jiuming He conceived and designed the experiments and revised the manuscript. Dan Liu designed and performed experiments, analyzed and interpreted the data, and drafted the manuscript. Jianpeng Huang and Shanshan Gao helped with the animal experiments. Hongtao Jin helped with manuscript editing. All authors have read and approved the final manuscript before submission.

### Conflicts of interest

The authors declare no conflict of interest.

### Appendix A. Supporting information

Supporting data to this article can be found online at <https://doi.org/10.1016/j.apsb.2022.03.018>.

### References

- Park HJ, Friston K. Structural and functional brain networks: from connections to cognition. *Science* 2013;**342**:1238411.
- Hassabis D, Maguire EA. The construction system of the brain. *Philos Trans R Soc Lond B Biol Sci* 2009;**364**:1263–71.
- Zhao R, Pollack GM. Regional differences in capillary density, perfusion rate, and P-glycoprotein activity: a quantitative analysis of regional drug exposure in the brain. *Biochem Pharmacol* 2009;**78**:1052–9.
- Pang X, Gao S, Ga M, Zhang J, Luo Z, Chen Y, et al. Mapping metabolic networks in the brain by ambient mass spectrometry imaging and metabolomics. *Anal Chem* 2021;**93**:6746–54.
- Shou WZ. Current status and future directions of high-throughput ADME screening in drug discovery. *J Pharm Anal* 2020;**10**:201–8.
- Guo HH, Feng CL, Zhang WX, Luo ZG, Zhang HJ, Zhang TT, et al. Liver-target nanotechnology facilitates berberine to ameliorate cardio-metabolic diseases. *Nat Commun* 2019;**10**:1981.
- Khan NU, Ni J, Ju X, Miao T, Chen H, Han L. Escape from abluminal LRP1-mediated clearance for boosted nanoparticle brain delivery and brain metastasis treatment. *Acta Pharm Sin B* 2021;**11**:1341–54.
- Bayet-Robert M, Morvan D, Chollet P, Barthomeuf C. Pharmacometabolomics of docetaxel-treated human MCF7 breast cancer cells provides evidence of varying cellular responses at high and low doses. *Breast Cancer Res Treat* 2010;**120**:613–26.
- Gao Y, Li W, Chen J, Wang X, Lv Y, Huang Y, et al. Pharmacometabolomic prediction of individual differences of gastrointestinal toxicity complicating myelosuppression in rats induced by irinotecan. *Acta Pharm Sin B* 2019;**9**:157–66.
- Wang D, Li D, Zhang Y, Chen J, Zhang Y, Liao C, et al. Functional metabolomics reveal the role of AHR/GPR35 mediated kynurenic acid gradient sensing in chemotherapy-induced intestinal damage. *Acta Pharm Sin B* 2021;**11**:763–80.
- Willmann JK, van Bruggen N, Dinkelborg LM, Gambhir SS. Molecular imaging in drug development. *Nat Rev Drug Discov* 2008;**7**:591–607.
- Logothetis NK. What we can do and what we cannot do with fMRI. *Nature* 2008;**453**:869–78.
- Lan Y, Bai P, Chen Z, Neelamegam R, Placzek MS, Wang H, et al. Novel radioligands for imaging sigma-1 receptor in brain using positron emission tomography (PET). *Acta Pharm Sin B* 2019;**9**:1204–15.
- Drake LR, Brooks AF, Stauff J, Sherman PS, Arteaga J, Koeppe RA, et al. Strategies for PET imaging of the receptor for advanced glycation endproducts (RAGE). *J Pharm Anal* 2020;**10**:452–65.
- Fox MD, Raichle ME. Spontaneous fluctuations in brain activity observed with functional magnetic resonance imaging. *Nat Rev Neurosci* 2007;**8**:700–11.
- Chen Y, Zheng T, Fan LI. Diagnosis of elderly brain atrophy patients with mental disorder according to their CT image. *Chin J Geriatric Heart Brain and Vessel Diseases* 2017;**19**:1299–301.
- Kolla NJ, Houle S. Single-photon emission computed tomography and positron emission tomography studies of antisocial personality disorder and aggression: a targeted review. *Curr Psychiatr Rep* 2019;**21**:24.
- Brahimaj BC, Kochanski RB, Pearce JJ, Guryildirim M, Gerard CS, Kocak M, et al. Structural and functional imaging in glioma management. *Neurosurgery* 2021;**88**:211–21.
- Ganesana M, Lee ST, Wang Y, Venton BJ. Analytical techniques in neuroscience: recent advances in imaging, separation, and electrochemical methods. *Anal Chem* 2017;**89**:314–41.
- Theodoridis G, Gika HG, Wilson ID. LC–MS-based methodology for global metabolite profiling in metabolomics/metabolomics. *Trac Trends Anal Chem* 2008;**27**:251–60.
- Gika HG, Theodoridis GA, Plumb RS, Wilson ID. Current practice of liquid chromatography–mass spectrometry in metabolomics and metabolomics. *J Pharm Biomed Anal* 2014;**87**:12–25.
- Castaing R, Slodzian G. Microanalyse par émission ionique secondaire. *J Microsc* 1962;1960.
- Castaing R, Slodzian G. Microanalysis using secondary ion emission. *J Mass Spectrom* 2021;**56**:e4800.
- Wiseman JM, Ifa DR, Venter A, Cooks RG. Ambient molecular imaging by desorption electrospray ionization mass spectrometry. *Nat Protoc* 2008;**3**:517–24.
- Takáts Z, Wiseman JM, Gologan B, Cooks RG. Mass spectrometry sampling under ambient conditions with desorption electrospray ionization. *Science* 2004;**306**:471–3.
- Swales JG, Dexter A, Hamm G, Nilsson A, Strittmatter N, Michopoulos F, et al. Quantitation of endogenous metabolites in mouse tumors using mass-spectrometry imaging. *Anal Chem* 2018;**90**:6051–8.
- Caprioli RM, Farmer TB, Gile J. Molecular imaging of biological samples: localization of peptides and proteins using MALDI-TOF MS. *Anal Chem* 1997;**69**:4751–60.
- Wang SS, Wang YJ, Zhang J, Sun TQ, Guo YL. Derivatization strategy for simultaneous molecular imaging of phospholipids and low-abundance free fatty acids in thyroid cancer tissue sections. *Anal Chem* 2019;**91**:4070–6.
- Zhao C, Xie P, Yong T, Wang H, Chung ACK, Cai Z. MALDI-MS imaging reveals asymmetric spatial distribution of lipid metabolites from bisphenol S-induced nephrotoxicity. *Anal Chem* 2018;**90**:3196–204.
- Wang Z, He B, Liu Y, Huo M, Fu W, Yang C, et al. *In situ* metabolomics in nephrotoxicity of aristolochic acids based on air flow-assisted desorption electrospray ionization mass spectrometry imaging. *Acta Pharm Sin B* 2020;**10**:1083–93.
- Wang Z, Fu W, Huo M, He B, Liu Y, Tian L, et al. Spatial-resolved metabolomics reveals tissue-specific metabolic reprogramming in diabetic nephropathy by using mass spectrometry imaging. *Acta Pharm Sin B* 2021;**11**:3665–77.
- Kleinriders A, Ferris HA, Reyzer ML, Rath M, Soto M, Manier ML, et al. Regional differences in brain glucose metabolism determined by imaging mass spectrometry. *Mol Metabol* 2018;**12**:113–21.
- Wang X, Hou Y, Hou Z, Xiong W, Huang G. Mass spectrometry imaging of brain cholesterol and metabolites with trifluoroacetic acid-enhanced desorption electrospray ionization. *Anal Chem* 2019;**91**:2719–26.
- He J, Sun C, Li T, Luo Z, Huang L, Song X, et al. A sensitive and wide coverage ambient mass spectrometry imaging method for functional metabolites based molecular histology. *Adv Sci* 2018;**5**:1800250.
- Li T, He J, Mao X, Bi Y, Luo Z, Guo C, et al. *In situ* biomarker discovery and label-free molecular histopathological diagnosis of lung cancer by ambient mass spectrometry imaging. *Sci Rep* 2015;**5**:14089.

36. Sun C, Li T, Song X, Huang L, Zang Q, Xu J, et al. Spatially resolved metabolomics to discover tumor-associated metabolic alterations. *Proc Natl Acad Sci U S A* 2019;**116**:52–7.
37. He J, Luo Z, Huang L, He J, Chen Y, Rong X, et al. Ambient mass spectrometry imaging metabolomics method provides novel insights into the action mechanism of drug candidates. *Anal Chem* 2015;**87**:5372–9.
38. Hamm G, Bonnel D, Legouffe R, Pamelard F, Delbos JM, Bouzom F, et al. Quantitative mass spectrometry imaging of propranolol and olanzapine using tissue extinction calculation as normalization factor. *J Proteomics* 2012;**75**:4952–61.
39. Taylor AJ, Dexter A, Bunch J. Exploring ion suppression in mass spectrometry imaging of a heterogeneous tissue. *Anal Chem* 2018;**90**:5637–45.
40. Swales JG, Strittmatter N, Tucker JW, Clench MR, Webborn PJH, Goodwin RJA. Spatial quantitation of drugs in tissues using liquid extraction surface analysis mass spectrometry imaging. *Sci Rep* 2016;**6**:37648.
41. Swales JG, Tucker JW, Strittmatter N, Nilsson A, Cobice D, Clench MR, et al. Mass spectrometry imaging of cassette-dosed drugs for higher throughput pharmacokinetic and biodistribution analysis. *Anal Chem* 2014;**86**:8473–80.
42. He J, Tang F, Luo Z, Chen Y, Xu J, Zhang R, et al. Air flow assisted ionization for remote sampling of ambient mass spectrometry and its application. *Rapid Commun Mass Sp* 2011;**25**:843–50.
43. Lv Y, Li T, Guo C, Sun C, Tang F, Huang L, et al. A high-performance bio-tissue imaging method using air flow-assisted desorption electrospray ionization coupled with a high-resolution mass spectrometer. *Chin Chem Lett* 2019;**30**:461–4.
44. He J, Huang L, Tian R, Li T, Sun C, Song X, et al. MassImager: a software for interactive and in-depth analysis of mass spectrometry imaging data. *Anal Chim Acta* 2018;**1015**:50–7.
45. Palmer A, Phapale P, Chernyavsky I, Lavigne R, Fay D, Tarasov A, et al. FDR-controlled metabolite annotation for high-resolution imaging mass spectrometry. *Nat Methods* 2017;**14**:57–60.
46. Lieberman JA, Bymaster FP, Meltzer HY, Deutch AY, Duncan GE, Marx CE, et al. Antipsychotic drugs: comparison in animal models of efficacy, neurotransmitter regulation, and neuroprotection. *Pharmacol Rev* 2008;**60**:358–403.
47. Amato D, Canneva F, Cumming P, Maschauer S, Groos D, Dahlmans JK, et al. A dopaminergic mechanism of antipsychotic drug efficacy, failure, and failure reversal: the role of the dopamine transporter. *Mol Psychiatry* 2020;**25**:2101–18.
48. Mombereau C, Kaupmann K, Froestl W, Sansig G, van der Putten H, Cryan JF. Genetic and pharmacological evidence of a role for GABA(B) receptors in the modulation of anxiety- and antidepressant-like behavior. *Neuropsychopharmacology* 2004;**29**:1050–62.
49. Zhou Y, Danbolt NC. Glutamate as a neurotransmitter in the healthy brain. *J Neural Transm (Vienna)* 2014;**121**:799–817.
50. Romanowska M, Komoszyński M. Adenosine–neurotransmitter and neuromodulator in the central nervous system. *Postepy Biochem* 2002;**48**:230–8.
51. Fredholm BB, Chen JF, Cunha RA, Svenningsson P, Vaugeois JM. Adenosine and brain function. *Int Rev Neurobiol* 2005;**63**:191–270.
52. Yu X, Franks NP, Wisden W. Sleep and sedative states induced by targeting the histamine and noradrenergic systems. *Front Neural Circ* 2018;**12**:4.
53. Parmentier R, Ohtsu H, Djebbara-Hannas Z, Valatx JL, Watanabe T, Lin JS. Anatomical, physiological, and pharmacological characteristics of histidine decarboxylase knock-out mice: evidence for the role of brain histamine in behavioral and sleep-wake control. *J Neurosci* 2002;**22**:7695–711.
54. Grossberg S. Acetylcholine neuromodulation in normal and abnormal learning and memory: vigilance control in waking, sleep, autism, amnesia and Alzheimer's disease. *Front Neural Circ* 2017;**11**:82.
55. Zhang Q, Liu Y, Wang H, Ma L, Xia H, Niu J, et al. The preventive effects of taurine on neural tube defects through the Wnt/PCP-Jnk-dependent pathway. *Amino Acids* 2017;**49**:1633–40.
56. Kanehisa M, Goto S, Sato Y, Kawashima M, Furumichi M, Tanabe M. Data, information, knowledge and principle: back to metabolism in KEGG. *Nucleic Acids Res* 2014;**42**:D199–205.
57. Hertz L, Zielke HR. Astrocytic control of glutamatergic activity: astrocytes as stars of the show. *Trends Neurosci* 2004;**27**:735–43.
58. Bak LK, Schousboe A, Waagepetersen HS. The glutamate/GABA-glutamine cycle: aspects of transport, neurotransmitter homeostasis and ammonia transfer. *J Neurochem* 2006;**98**:641–53.
59. Kumar J, Liddle EB, Fernandes CC, Palaniyappan L, Hall EL, Robson SE, et al. Glutathione and glutamate in schizophrenia: a 7T MRS study. *Mol Psychiatry* 2020;**25**:873–82.
60. Fernie AR, Carrari F, Sweetlove LJ. Respiratory metabolism: glycolysis, the TCA cycle and mitochondrial electron transport. *Curr Opin Plant Biol* 2004;**7**:254–61.
61. Akram M. Citric acid cycle and role of its intermediates in metabolism. *Cell Biochem Biophys* 2014;**68**:475–8.
62. Hashimoto K, Bruno D, Nierenberg J, Marmar CR, Zetterberg H, Blennow K, et al. Abnormality in glutamine-glutamate cycle in the cerebrospinal fluid of cognitively intact elderly individuals with major depressive disorder: a 3-year follow-up study. *Transl Psychiatry* 2016;**6**:e744.
63. Zarrindast M, Rostami P, Sadeghi-Hariri M. GABA(A) but not GABA(B) receptor stimulation induces antianxiety profile in rats. *Pharmacol Biochem Behav* 2001;**69**:9–15.
64. Michaeli S, Fait A, Lagor K, Nunes-Nesi A, Grillich N, Yellin A, et al. A mitochondrial GABA permease connects the GABA shunt and the TCA cycle, and is essential for normal carbon metabolism. *Plant J* 2011;**67**:485–98.
65. Pastorino JG, Hoek JB. Hexokinase II: the integration of energy metabolism and control of apoptosis. *Curr Med Chem* 2003;**10**:1535–51.
66. Fahy E, Subramaniam S, Brown HA, Glass CK, Merrill Jr AH, Murphy RC, et al. A comprehensive classification system for lipids. *J Lipid Res* 2005;**46**:839–61.
67. Gibellini F, Smith TK. The Kennedy pathway—*de novo* synthesis of phosphatidylethanolamine and phosphatidylcholine. *IUBMB Life* 2010;**62**:414–28.
68. Gouvêa-Junqueira D, Falvella ACB, Antunes ASLM, Seabra G, Brandão-Teles C, Martins-de-Souza D, et al. Novel treatment strategies targeting myelin and oligodendrocyte dysfunction in schizophrenia. *Front Psychiatry* 2020;**11**:379.
69. Bowers M, Liang T, Gonzalez-Bohorquez D, Zocher S, Jaeger BN, Kovacs WJ, et al. FASN-dependent lipid metabolism links neurogenic stem/progenitor cell activity to learning and memory deficits. *Cell Stem Cell* 2020;**27**:98–109.
70. Sun WY, Tyurin VA, Mikulska-Ruminska K, Shrivastava IH, Anthonyamuthu TS, Zhai YJ, et al. Phospholipase iPLA2 $\beta$  averts ferroptosis by eliminating a redox lipid death signal. *Nat Chem Biol* 2021;**17**:465–76.
71. Luo X, Gong HB, Gao HY, Wu YP, Sun WY, Li ZQ, et al. Oxygenated phosphatidylethanolamine navigates phagocytosis of ferroptotic cells by interacting with TLR2. *Cell Death Differ* 2021;**28**:1971–89.